CrossMark

Nonlinear Buckling Analysis of H-Type Honeycombed Composite Column with Rectangular Concrete-Filled Steel Tube Flanges

Jing Ji[1,2] · Zhichao Xu[1] · Liangqin Jiang[1] · Chaoqing Yuan[1] · Yunfeng Zhang[1] · Lijian Zhou[1] · Shilong Zhang[1]

Abstract

This paper was concerned with the nonlinear analysis on the overall stability of H-type honeycombed composite column with rectangular concrete-filled steel tube flanges (STHCC). The nonlinear analysis was performed using ABAQUS, a commercially available finite element (FE) program. Nonlinear buckling analysis was carried out by inducing the first buckling mode shape of the hinged column to the model as the initial imperfection with imperfection amplitude value of $L/1000$ and importing the simplified constitutive model of steel and nonlinear constitutive model of concrete considering hoop effect. Close agreement was shown between the experimental results of 17 concrete-filled steel tube (CFST) specimens and 4 I-beams with top flanges of rectangular concrete-filled steel tube (CFSFB) specimens conducted by former researchers and the predicted results, verifying the correctness of the method of FE analysis. Then, the FE models of 30 STHCC columns were established to investigate the influences of the concrete strength grade, the nominal slenderness ratio, the hoop coefficient and the flange width on the nonlinear stability capacity of SHTCC column. It was found that the hoop coefficient and the nominal slenderness ratio affected the nonlinear stability capacity more significantly. Based on the results of parameter analysis, a formula was proposed to predict the nonlinear stability capacity of STHCC column which laid the foundation of the application of STHCC column in practical engineering.

Keywords Nonlinear buckling · H-type honeycombed composite column · ABAQUS · Concrete-filled steel tube (CFST) flange · Stability bearing capacity

1 Introduction

With the revitalization of the old industrial base in Northeast China, jacketing structure, a new construction technique used to add stories to the existing buildings, has been drawing lots of attentions (Ji et al. 2018). Jacketing structure includes mainly two forms: synergy and separation (Zheng and Ji 2008a, b). The separating jacketing structure is separated from the original building to independently bear and transfer the load from the adding stories to the new foundation. Hence, the separating jacketing structure is suitable for storey adding of low existing buildings. Although steel structure has been widely applied in industrial and civilian buildings because of its light weight, high bearing capacity, and good economic (Zhang et al. 2014; Patton and Singh 2017), it cannot meet the requirements of jacketing structure which needs to span over the existing building with larger span length. For this reason, a new form of steel frame structure is proposed which connects composite column (i.e., the H type honeycomb composite column (Ji et al. 2017) with concrete-filled rectangular steel tube flanges) with composite beam (i.e., the I-shaped honeycomb composite beam with concrete-filled rectangular steel tube flanges) using integral joint. In order to reduce the deflection of the composite beam, the prestressed reinforcements can be located in the lower steel tube flange, pre-tensioned and anchored at the end of the integral joint.

The rectangular steel tube flange of this kind of columns is filled with concrete, under the action of axial load the steel tube exerts lateral restraint on the compressive concrete, which makes the concrete in the three direction compressive stress state, retards the occurrence and development of its longitudinal microfracture, thereby improves its compressive strength

✉ Jing Ji
jijing1977@163.com

[1] Heilongjiang Key Laboratory of Disaster Prevention, Mitigation and Protection Engineering, College of Civil Engineering, Northeast Petroleum University, Daqing, China

[2] Department of Civil and Environmental Engineering, The Hong Kong Polytechnic University, Hong Kong, China

and compression deformation ability. Then, with the support of the concrete, the geometric stability of the steel tube wall is enhanced and the instability mode of the steel tube is changed, thus the bearing capacity of the steel tube is improved. The concrete-filled steel tube uses the interaction between the steel tube and concrete, namely the restraining effect of the steel tube on the concrete makes the concrete under the state of complex stress, as a result, the strength of concrete is improved, and the plasticity and toughness are greatly improved. At the same time, the local buckling can be avoided or delayed because of the existence of concrete. In addition, during the construction process of CFST, the steel tube can also serve as a template for pouring its core concrete. In short, CFST is formed by combination between steel tube and concrete, which not only can make up for the shortcomings of the two materials, but also bring the advantages of two materials into full play. Furthermore, the honeycombed web connecting the two CFST columns can reduce the self-weight of the composite columns effectively and make the building beautiful when exposed to the outside. The rigidity of the cross section is no longer constant along the longitudinal direction after opening in the web, but for a honeycomb column with regular openings, the stiffness changes are characterized by repeated regularity because of the overall stiffness of each opening unit is equal. Therefore, the whole column can still be regarded as a column of equal stiffness from the macroscopic point of view.

Numerous researches have been conducted on I-beam with steel tube flanges or CFST flanges. Hassanein and Silvestre (2013) studied the lateral–distortional buckling of hollow steel tube flange plate girders with slender unstiffened webs (HTFPG). The good agreement between the obtained experimental results of the buckling capacity with the predictions provided by European code verified the rationality of method provided by the code. Then, they provided some design suggestions. Liang (2016) in our group carried out the experimental study on the overall stability of I-beams with rectangular CFST flange and proposed a formula to predict their ultimate bending moment. With the help of 1stOpt software, the non-dimensional critical moment formula of the lateral-torsional buckling of cantilever beam with tip lateral elastic brace is obtained by Zhang et al. (2016) based on stability theory. Then, the accuracy of the formula is verified by ADINA finite element software. The studies on the CFST composite columns are mainly focused on the conventional CFST columns and the latticed columns. Lama and Gardner (2008) conducted axial compression tests on 16 hollow stainless steel tube and concrete-filled stainless steel tube columns to investigate the influences of different parameters on the bearing capacity of the columns and established a formula to predict the bearing capacity of the column. The correctness of the proposed formula was verified through comparing with the predictions calculated by EC4 and ACI. Ellobody and Ghazym (2012) carried out the experimental investigation of axially and eccentrically

loaded plain and fibre rein-forced (FR) concrete-filled stainless steel circular tubular columns. The test ultimate loads were compared with the design ultimate loads calculated using the Eurocode 4 for composite columns and the results showed that the EC4 accurately predicted the ultimate loads of axially loaded concrete-filled stainless steel circular tubular columns, but were quite conservative for predicting the ultimate loads of the eccentrically loaded columns. Lastly, the test results provide useful information regarding the behaviour of FR concrete-filled stainless steel columns. Zhong (2010) studied the stability of CFST latticed columns based on stability theory, derived a calculation method of the equivalent slenderness ratio and proposed a formula to predict the stability bearing capacity of the column. Zhou (2012) conducted the axial compression, bending and pseudo-static tests on square CFST columns to investigate the influence of structural form on the bearing capacity and the seismic performance of the column and proposed a formula to estimate the bearing capacity of the column. Yang et al. (2016) carried out the experimental investigation to study the effects of slenderness ratio, eccentricity and column slope on the load-carrying capacities and failure modes of variable and uniform concrete filled steel tubular (CFST) latticed columns under axial and eccentric compression. The results clearly showed that all the CFST latticed columns with variable cross section exhibited an overall failure, which is similar to that of CFST latticed columns with a uniform cross section. For the eccentrically compressed variable CFST latticed columns, the strain of the columns at the loading side, as well as the difference in the strain, increases from the bottom to the cap, and a more significant increase in strain is observed in the cross section closer to the column cap. Our group carried out the eigenvalue analysis of 18 H-type honeycomb composite columns with rectangular concrete-filled steel tube flanges (STHCC) (Ji et al. 2017), introduced the influence factor β of concrete and established a formula to predict the eigenvalue buckling load of this kind of composite columns based on Euler formula.

The STHCC column not only exhibits the characteristics of double-legged CFST latticed column, but also yields the weak stability of H-type honeycombed steel column. Up to now, there have been few researches on the nonlinear buckling analysis of STHCC, and the corresponding design methods are not perfect. Therefore it is significant to conduct the nonlinear buckling analysis of the STHCC. Based on the former eigenvalue analysis (Ji et al. 2017) developed by our group, 30 finite element models of STHCC are established by using finite element software ABAQUS. The influences of different parameters including the concrete strength grade, the nominal slenderness ratio, the hoop coefficient and the flange width on the nonlinear buckling capacity of STHCC columns are investigated. In addition, a formula is proposed to predict the nonlinear buckling load of STHCC column through regression analysis based on the results of parameter study.

2 Specimens Design

In order to study the nonlinear overall stability of STHCC, the concrete strength grade f k cu, the nominal slenderness ratio λ_t, the hoop coefficients ξ and the flange width h_1 are selected as the main parameters. 30 STHCC specimens with different parameters are designed. The specific parameters of each specimen are listed in Table 1. The slenderness ratio of the composite columns is calculated according to the equation of the nominal slenderness ratio of the steel column (Eq. 1) proposed by Strength of Materials (James and Barry 2011) and the physical meaning of each symbol can be referred to the design code for steel structure (BS

EN 1993-1-1 2005). Due to both ends of the specimen are hinged, the calculated length factor μ is equal to 1 and the calculated length l_0 is l. The honeycomb web is formed by opening holes on steel webs with the diameter to height ratio d/h_w of 0.7, and the space between two holes to height ratio s/h_w of 0.3. The connection between the flange and web is welded. The section size of the specimen is shown in Fig. 1, and the three-dimensional figure of the specimen is shown in Fig. 2.

$$\lambda_t = \frac{l_0}{i} = \frac{l_0}{\sqrt{\left(I_s + 0.8\frac{E_c}{E_s}I_c\right) \Big/ \left(A_s + 0.8\frac{E_c}{E_s}A_c\right)}} \qquad (1)$$

Table 1 Parameters of 30 STHCC specimens

No.	Section size $h_w \times h_1 \times b \times t_1 \times t_2$ (mm⁵)	Actual length L (m)	Nominal slenderness ratios λ_t	Area of flange steel tube A_s (mm²)	Area of concrete A_c (mm²)	Hoop coefficient ξ	Concrete strength grade f k cu (MPa)
C-1	$380 \times 100 \times 200 \times 10 \times 20$	11	203.20	11200	28800	6.70	30
C-2	$380 \times 100 \times 200 \times 10 \times 20$	11	203.31	11200	28800	5.01	40
C-3	$380 \times 100 \times 200 \times 10 \times 20$	11	203.38	11200	28800	4.01	50
C-4	$380 \times 100 \times 200 \times 10 \times 20$	11	203.45	11200	28800	3.27	60
C-5	$380 \times 100 \times 200 \times 10 \times 20$	11	203.53	11200	28800	2.80	70
C-6	$380 \times 100 \times 200 \times 10 \times 20$	6	110.84	11200	28800	6.70	30
C-7	$380 \times 100 \times 200 \times 10 \times 20$	7	129.31	11200	28800	6.70	30
C-8	$380 \times 100 \times 200 \times 10 \times 20$	8	147.78	11200	28800	6.70	30
C-9	$380 \times 100 \times 200 \times 10 \times 20$	9	166.26	11200	28800	6.70	30
C-10	$380 \times 100 \times 200 \times 10 \times 20$	10	184.73	11200	28800	6.70	30
C-11	$380 \times 100 \times 200 \times 10 \times 20$	12	221.68	11200	28800	6.70	30
C-12	$380 \times 100 \times 200 \times 10 \times 20$	13	240.15	11200	28800	6.70	30
C-13	$380 \times 100 \times 200 \times 11 \times 20$	11	201.33	12232	27768	7.60	30
C-14	$380 \times 100 \times 200 \times 12 \times 20$	11	199.81	13248	26752	8.54	30
C-15	$380 \times 100 \times 200 \times 13 \times 20$	11	198.59	14248	25752	9.54	30
C-16	$380 \times 100 \times 200 \times 14 \times 20$	11	197.60	15232	24768	10.61	30
C-17	$380 \times 100 \times 200 \times 15 \times 20$	11	196.81	16200	23800	11.74	30
C-18	$380 \times 100 \times 200 \times 16 \times 20$	11	196.20	17152	22848	12.96	30
C-19	$380 \times 120 \times 200 \times 10 \times 20$	11	196.68	12000	36000	5.75	30
C-20	$380 \times 120 \times 200 \times 10 \times 20$	12	214.56	12000	36000	5.75	30
C-21	$380 \times 120 \times 200 \times 10 \times 20$	13	232.44	12000	36000	5.75	30
C-22	$380 \times 150 \times 200 \times 10 \times 20$	11	189.23	13200	46800	4.87	30
C-23	$380 \times 150 \times 200 \times 10 \times 20$	12	206.43	13200	46800	4.87	30
C-24	$380 \times 150 \times 200 \times 10 \times 20$	13	223.64	13200	46800	4.87	30
C-25	$380 \times 170 \times 200 \times 10 \times 20$	11	185.35	14000	54000	4.47	30
C-26	$380 \times 170 \times 200 \times 10 \times 20$	12	202.20	14000	54000	4.47	30
C-27	$380 \times 170 \times 200 \times 10 \times 20$	13	219.05	14000	54000	4.47	30
C-28	$380 \times 200 \times 200 \times 10 \times 20$	11	180.66	15200	64800	4.05	30
C-29	$380 \times 200 \times 200 \times 10 \times 20$	12	197.08	15200	64800	4.05	30
C-30	$380 \times 200 \times 200 \times 10 \times 20$	13	213.50	15200	64800	4.05	30

The yield strength of steel is $f_y = 345$Mpa, the elastic modulus of steel is $E_s = 2.1 \times 10^5$ Mpa, f_{ck} is the standard value of axial compressive strength for concrete
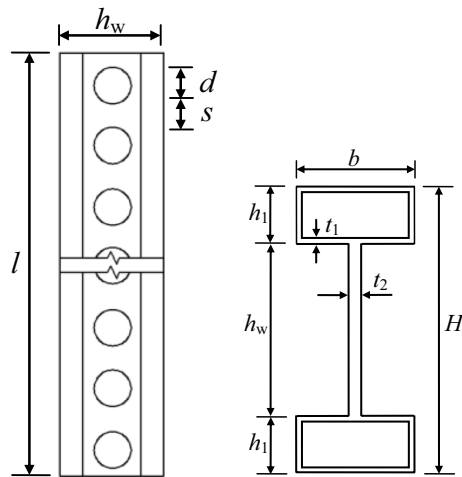
Fig. 1 The section size of H-type steel column with honeycombed web and hollow flanges
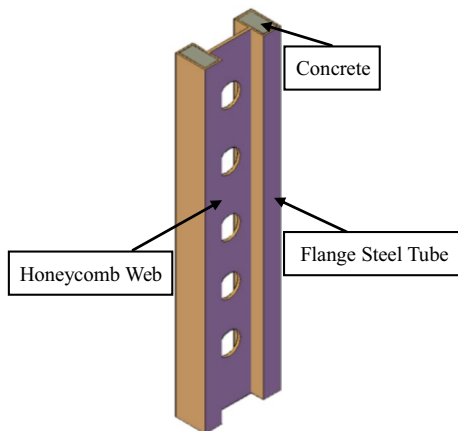
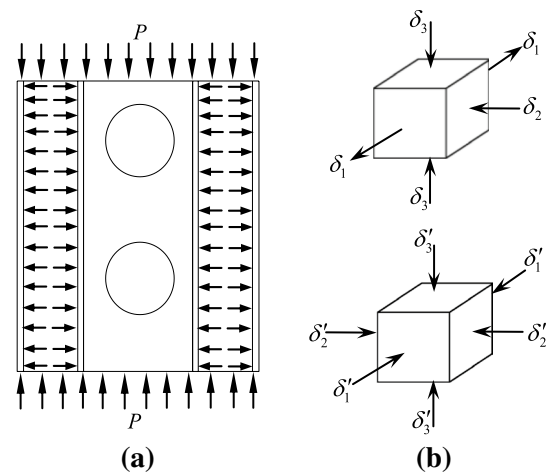**Fig. 2** The three-dimensional figure of specimen

Fig. 3 Three-dimensional stress states of steel tube and concrete

3 Stress Mechanism

CFST flanges are formed by filling concrete into the hollow flange steel tube. Figure 3 shows the three-dimensional stress state of the steel tube as well as the inner concrete. Under the longitudinal axial compression P, the longitudinal compressive strain can be calculated as follows:

$$\varepsilon_{1s} = \mu_s \varepsilon_3 \; ; \varepsilon_{1c} = \mu_c \varepsilon_3 \tag{2}$$

where, μ_s and μ_c are the Poisson's ratio of steel and concrete respectively. ε_{1s} and ε_{1c} are transverse strain of steel and concrete respectively.

The relationship between the Poisson's ratio of steel and concrete of the CFST flange of STHCC specimen was changed during the loading process. At the beginning, the Poisson' ratio of concrete was smaller than that of the steel (i.e., $\mu_c < \mu_s$); when the longitudinal compressive stress of the

steel reached its proportional limit (i.e., $\delta_3 \approx f_p$), the Poisson' ratio of concrete was similar with that of the steel ($\mu_c \approx \mu_s$); then, with further increase of the compression load P, the stress of the steel exceeded its proportional limit (i.e., $\delta_3 > f_p$), in this case, the Poisson' ratio of concrete became larger than that of the steel (i.e., $\mu_c > \mu_s$), hence, the corresponding strain of concrete was also larger than that of steel according to Eq. 2 (i.e., $\varepsilon_{1c} > \varepsilon_{1s}$), which mean that the expansion of core concrete was larger than that of the steel tube. Therefore, the core concrete was restrained by the steel tube and its lateral expansion was hindered. The interaction force generated between the steel tube and the core concrete, as shown in Fig. 3a. The longitudinal compression stress (δ_3), the radial compression stress (δ_2), the circumferential tension stress (δ_1) of the steel tube and the longitudinal, radial and circumferential compression stress of core concrete (δ_3', δ_2', δ_1') are presented in Fig. 3b. Due to the deformation of the steel tube caused by the hoop force, the hoop force was significantly reduced in the middle of the edge, as shown in Fig. 4a. In addition, the circumferential shear stress τ and the normal stress pointing to the honeycomb of web were produced when subjected to compression P, as shown in Fig. 4b.

When the CFST is subjected to axial compression, the hoop effect would occur. The steel tube and the core concrete are under the three-directional stress state which is different from the uniaxial compression state, and the material properties are changed at the same time. With the increase of the hoop effect, the compressive strength of concrete increases gradually, and similarly, the elastic modulus. In addition, the plastic deformation ability of concrete also increases obviously and the concrete transforms from brittle material to plastic material. In addition, the local stability of CFST flange is improved because of supporting provided by the core concrete, hence the yield strength of steel can be fully utilized.
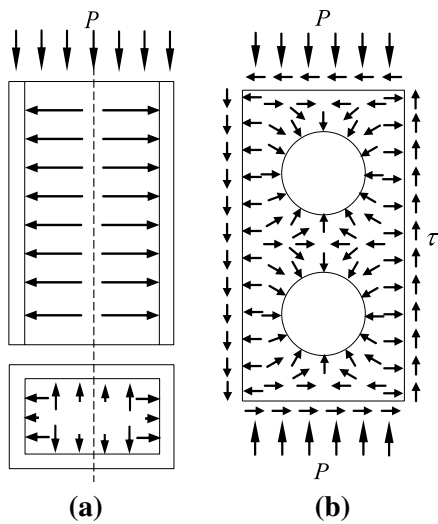
Fig. 4 Stress distribution state of CFST flange and web. **a** CFST flange, **b** web

4 Finite Element Model and Model Verification

4.1 Constitutive Models of Steel and Concrete

4.1.1 Constitutive Model of Concrete

The nonlinear constitutive model of concrete proposed by Han (2016) considering the hoop effect is adopted in present research as shown in Fig. 5a.

The stress–strain relationship of core concrete of CFST under compression is expressed as follows:

$$y = \begin{cases} 2 \cdot x - x^2 & (x \le 1) \\ \frac{x}{\beta_0 \cdot (x-1)^\eta + x} & (x > 1) \end{cases} \tag{3}$$

$x = \frac{\varepsilon}{\varepsilon_0}, y = \frac{\delta}{\delta_0}$, $\delta_0 = f_c$(N/mm^2). The constant ε_0 can be obtained from formulae (4) and (5).

$$\varepsilon_c = (1300 + 12.5 \cdot f_c) \cdot 10^{-6} \tag{4}$$

$$\varepsilon_0 = \varepsilon_c + 800 \cdot \xi^{0.2} \cdot 10^{-6} \tag{5}$$

where, ξ is hoop effect coefficient which can be calculated by formula (6).

$$\xi = \frac{A_s f_y}{A_c f_{ck}} \tag{6}$$

The coefficients (β_0 and η) in formula 1 can be calculated by formulae (7) and (8) as follows.

$$\eta = \begin{cases} 2 & \text{Circular CFST} \\ 1.6 + 1.5/x & \text{Rectangular CFST} \end{cases} \tag{7}$$

$$\beta_0 = \begin{cases} (2.36 \times 10^{-5})^{[0.25 + (\xi - 0.5)^7]} \cdot f_c^{0.5} \cdot 0.5 \ge 0.12 & \text{Circular CFST} \\ \frac{f_c^{0.1}}{1.2\sqrt{1+\xi}} & \text{Rectangular CFST} \end{cases} \tag{8}$$

The stress–strain relationship of core concrete of CFST under tension is expressed as follows:

$$y = \begin{cases} 1.2 \cdot x - 0.2 \cdot x^6 & (x \le 1) \\ \frac{x}{0.31 \cdot \delta_p^2 \cdot (x-1)^{1.7} + x} & (x > 1) \end{cases} \tag{9}$$

where, $x = \frac{\varepsilon_c}{\varepsilon_p}$; $y = \frac{\delta_c}{\delta_p}$; $\delta_p = 0.26 \cdot (1.25 \cdot f_c)^{2/3}$; $\varepsilon_p = 43.1 \cdot \delta_p (\mu\varepsilon)$.

The damage factor is inputted into concrete constitutive model in ABAQUS software to form the concrete damage plasticity model, which are calculated by the formula (10) and (11) from the reference (Li 2011).
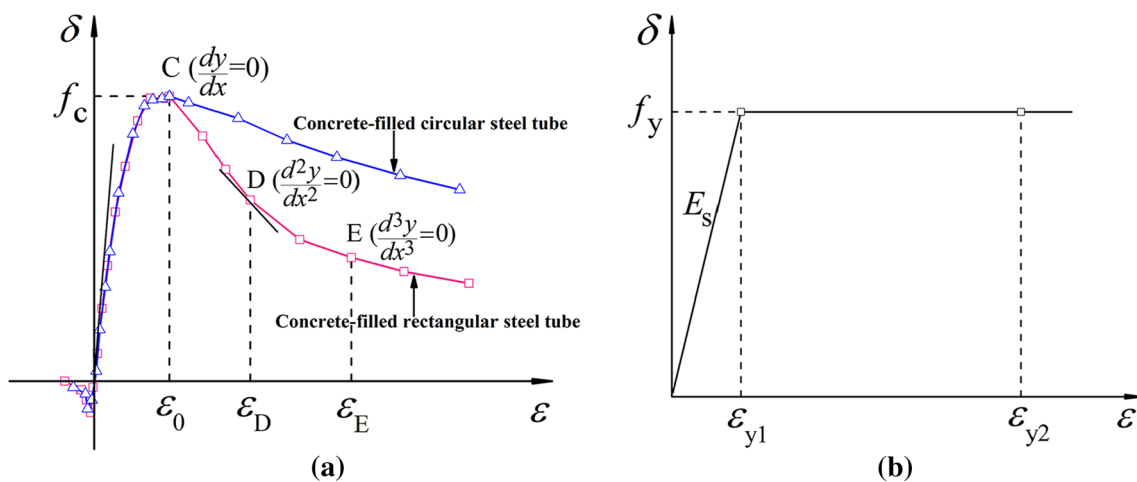

Fig. 5 Constitutive models of concrete and steel. **a** Constitutive model of concrete (Han 2016), **b** Constitutive model of steel

$$d_c = 1 - \frac{(\delta_c + 2\delta_{c_0})}{E_c(2\delta_{c_0}/E_c + \varepsilon_c)}(d_c \geq 0) \tag{10}$$

$$d_t = 1 - \frac{(\delta_t + \delta_{t_0})}{E_c(\delta_{t_0}/E_c + \varepsilon_t)}(d_t \geq 0) \tag{11}$$

where, d_c, d_t is the compression damage factor and the tensile damage factor, respectively; E_c is the initial elastic modulus of concrete (Han 2016).

4.1.2 Constitutive Model of Steel

The stress–strain curve of steel is generally divided into five stages: elastic, elastic–plastic, plastic, strengthening and second plastic flow. The STHCC columns conducted in this paper are all long columns hence the strengthening stage of steel can be neglected. Therefore, the ideal elastoplastic constitutive model shown in Fig. 5b is adopted.

4.2 Finite Element Model

ABAQUS software (ABAQUS Inc. 2006) is used to establish the finite element models of STHCC specimens. In order to obtain the stress distributions of steel and concrete, 8-node brick elements (C3D8R) with three translation degrees of freedom at each node were adopted to simulate steel and concrete. Through arranging the hexahedral seeds, the fine mesh of the composite columns was achieved. The plastic damage model was used to describe the material property of concrete which was achieved by inputting the coordinates of the points in the constitutive model of concrete as shown in Fig. 5a. The interface between steel tube and concrete is simulated by contact element, which is composed of normal contact and tangential bond-slip. The hard contact in ABAQUS is chosen as the normal contact behavior between the steel tube and concrete, and the tangential contact is modeled by the Coulomb friction model, and the friction coefficient is 0.25.

Both the top and bottom ends of the columns were fixed against all displacement except for the vertical displacement at the loaded end and all rotation angles to realize hinge connection. The axial load was applied on the top of column through the line displacement of the reference point RP. The FE model of one typical specimen is shown in Fig. 6. This initial geometric imperfection of the column specimens was simulated in the model as the first buckling mode shape of the hinged column multiplied by an amplification factor. Hence, a previous eigenvalue analysis of the model was conducted. Once the initial shape of the column was obtained, it was imported to the model as the initial imperfection. The imperfection amplitude value of $L/1000$ employed by the majority of researchers for the amplification factor was used. The nonlinear buckling simulation analysis of composite columns was carried out by using Riks method.

4.3 Model Verification

According to the above method, the nonlinear buckling analyses of 17 CFST columns (Han 2016) and 4 CFSFB (Ren 2015; Liang 2016) were conducted, and the parameters of them and the overall stability bearing capacity obtained by test (N_{ue}) and nonlinear buckling simulation analysis (N_{usn}) are listed in Tables 2 and 3.

The comparison of the load–displacement curves obtained by experiments and FE simulations for 21 specimens is shown in Fig. 7.

It can be seen from Fig. 7, Tables 2 and 3 that the FE outcomes obtained by adopting Han's constitutive model of concrete consist better with the experimental results in forms of load–displacement curves and overall stability capacity when compared with those obtained by using the concrete constitutive models proposed by GB (2014) or Yu (2003). Therefore, the concrete constitutive model proposed by Han is adopted to conduct FE analysis. In addition, the feasibility of the modeling method proposed above for the buckling analysis of CFST columns and CFSFB is also verified. The STHCC specimens in this paper are similar to CFST columns and CFSFB, hence the same modeling method can be used to analyze the overall stability of STHCC specimens.

5 Nonlinear Buckling Analysis of the STHCC

Nonlinear buckling analysis of 30 STFCC columns was carried out by using ABAQUS finite element software. The relationships between the vertical load and horizontal
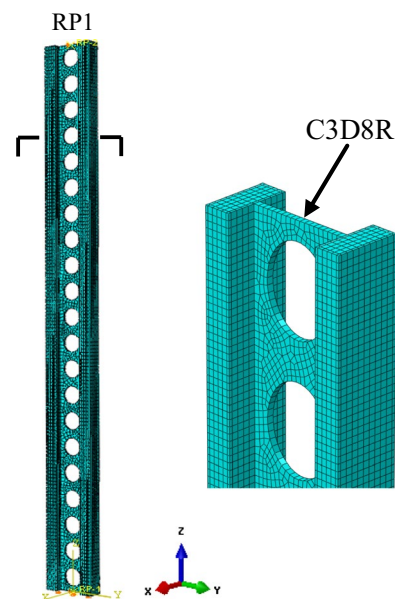

Fig. 6 FE model of specimen

Table 2 The comparison of stability bearing capacity of 17 CFST columns

No.	Size of specimen ($D/B \times t \times L$) (mm^4)	Test value N_{ue} (kN)	GB (2014) N_{usn} (kN)	$\left\|\frac{N_{usn}-N_{ue}}{N_{ue}}\right\|$ (%)	Yu and Ding (2003) N_{usn} (kN)	$\left\|\frac{N_{usn}-N_{ue}}{N_{ue}}\right\|$ (%)	Han (2016) N_{usn} (kN)	$\left\|\frac{N_{usn}-N_{ue}}{N_{ue}}\right\|$ (%)	
Sc154-1	108×4.5×4158	342.0	263.23	23.03	274.57	19.72	287.10	19.12	Han (2016)
Sc154-2	108×4.5×4158	292.0	263.23	9.85	274.57	5.97	287.10	1.71	
Sc154-3	108×4.5×4158	298.0	287.26	3.60	303.47	1.84	301.08	1.02	
Sc154-4	108×4.5×4158	280.0	287.26	2.59	303.47	8.38	301.08	7.00	
Sc149-1	108×4.5×4023	318.0	315.28	0.86	316.21	0.56	319.41	0.44	
Sc149-2	108×4.5×4023	320.0	315.28	1.48	316.21	1.18	319.41	0.18	
Sc141-1	108×4.5×3807	350.0	339.62	3.00	343.63	1.82	348.39	0.46	
Sc141-2	108×4.5×3807	370.0	339.62	8.21	343.63	7.13	348.39	6.20	
Sc130-1	108×4.5×3510	400.0	396.32	0.92	407.52	1.88	398.71	0.32	
Sc130-2	108×4.5×3510	390.0	396.32	1.62	407.52	4.49	398.71	2.19	
Sc130-3	108×4.5×3510	440.0	415.41	5.59	413.21	6.09	416.15	5.73	
scz1-1-1	120×3.84×2602	753.2	764.12	1.45	774.12	2.78	841.88	10.53	Han (2016)
scz1-1-2	120×3.84×2602	833.0	764.12	8.27	774.12	7.07	841.88	1.05	
scz1-1-3	120×3.84×2602	980.0	879.56	10.25	882.83	9.92	987.58	0.77	
scz1-2-1	140×3.84×2558	1048.6	1079.03	2.90	1066.31	1.69	1095.33	4.27	
scz1-2-2	140×3.84×2558	1127.0	959.25	14.89	956.33	15.14	1056.25	6.70	
scz1-2-3	140×3.84×2558	1323.0	1276.31	3.53	1274.31	3.68	1381.37	4.22	

Table 3 The comparison of stability bearing capacity of 4 CFSFB

No.	Section size $h_w \times h_1 \times b_1 \times b_2 \times t_1 \times t_2 \times t_3 \times L$ (mm^8)	Test value N_{ue} (kN)	GB (2014) N_{usn} (kN)	$\left\|\frac{N_{usn}-N_{ue}}{N_{ue}}\right\|$ (%)	Yu and Ding (2003) N_{usn} (kN)	$\left\|\frac{N_{usn}-N_{ue}}{N_{ue}}\right\|$ (%)	Han (2016) N_{usn} (kN)	$\left\|\frac{N_{usn}-N_{ue}}{N_{ue}}\right\|$ (%)	
L-2	256.72×39.74×79.56×79.62×2.58×4.70×4.70×2800	142.56	133.28	6.51	136.51	4.24	149.31	4.73	Ren (2015)
CFSFB-1	252.30×50.90×71.38×68.20×3.40×4.90×5.30×4120	86.66	67.93	21.61	74.52	14.00	90.31	4.21	Liang (2016)
CFSFB-2	263.40×40.30×80.10×82.76×3.40×5.60×5.40×4120	105.86	79.23	25.16	84.95	19.75	103.53	2.20	
CFSFB-3	254.72×50.08×100.04×99.72×3.30×4.80×5.44×4120	103.61	89.71	13.42	88.13	14.94	108.46	4.68	
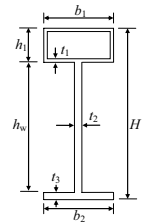
displacement in mid-height of the specimens were extracted. The influences of the concrete strength grade, the nominal slenderness ratio, the hoop coefficient and the flange width on the nonlinear stability bearing capacity of composite columns were investigated.
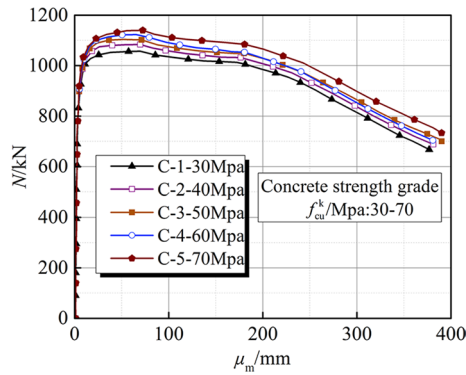
5.1 Concrete Strength Grade (f_{cu}^k)

The load–displacement (N-μ_m) curves of STHCC specimens with different concrete strength grades (i.e., 30, 40, 50, 60 and 70) are shown in Fig. 8, and the stability bearing capacity is listed in Table 4. It can be seen from Fig. 8 that with the increase of the concrete strength grade, the stability bearing capacity of the column increases gradually. However,

(a)   (b)   (c)

(d)   (e)   (f)

(g)   (h)   (i)

(j)   (k)   (l)

(m)   (n)   (o)
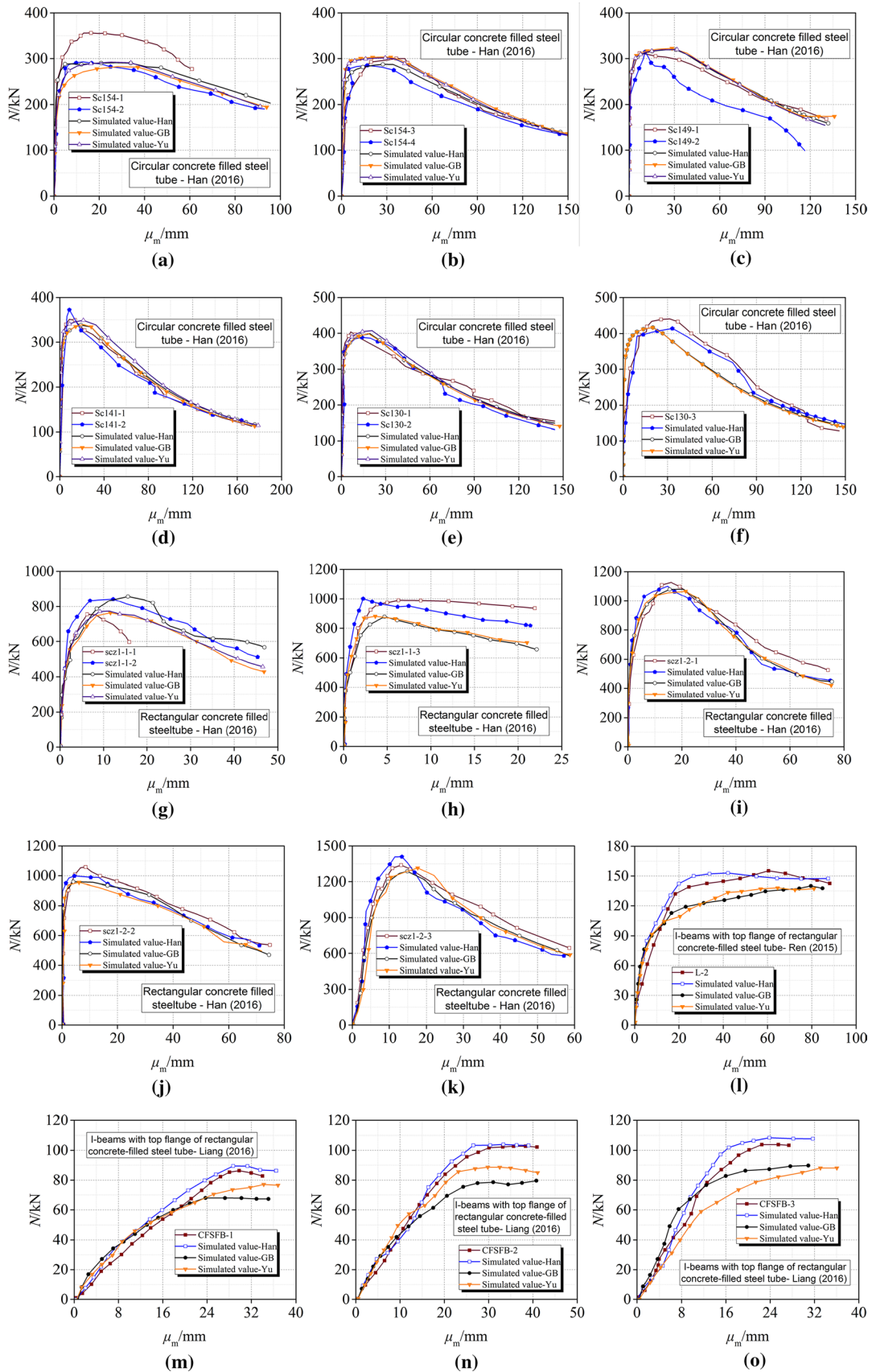
Fig. 7 Load-displacement curves of specimens. **a** Sc154-1 and Sc154-2, **b** Sc154-3 and Sc154-4, **c** Sc149-1 and Sc149-2, **d** Sc141-1 and Sc141-2, **e** Sc130-1 and Sc130-2, **f** Sc130-3, **g** scz1-1-1 and scz1-1-2, **h** scz1-1-3, **i** scz1-2-1, **j** scz1-2-2, **k** scz1-2-3, **l** L-2, **m** CFSFB-1, **n** CFSFB-2, **o** CFSFB-3

Fig. 8 The load–displacement (N-μ_m) curves of STHCC specimens with different concrete strength grades

Table 4 The stability bearing capacity of specimens

No.	C-1	C-2	C-3	C-4	C-5
f k cu (MPa)	30	40	50	60	70
N_{usn} (kN)	1058.83	1085.83	1104.18	1114.53	1139.27
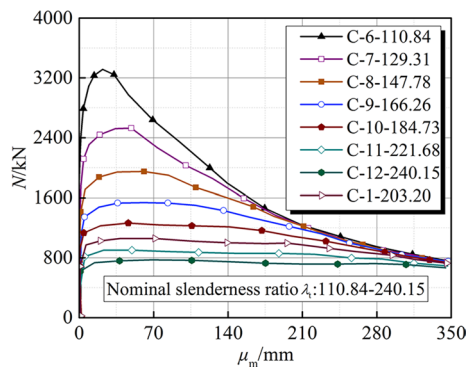
Fig. 9 The load–displacement (N-μ_m) curves of STHCC specimens with different nominal slenderness ratios

the increase of the stability bearing capacity with concrete strength is not significant. It can be seen from Table 4 that the stability bearing capacity increases from 1058.83 to 1139.27 kN with an increase of 7.60% when the concrete strength grade increase from 30 to 70. Hence, through increasing the concrete strength grade to improve the stability bearing capacity of the column is limited.
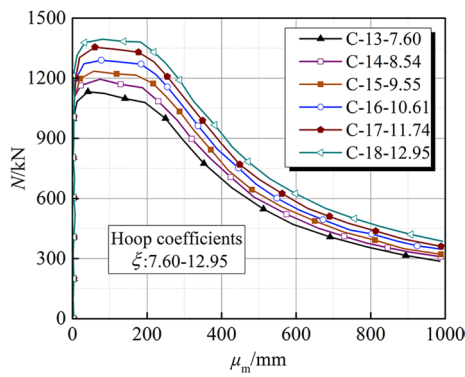
5.2 Nominal Slenderness Ratio (λ_t)

Figure 9 depicts the predicted load–displacement (N-μ_m) curves of the STHCC specimens with different nominal slenderness ratios (i.e., 110.84, 129.31, 147.78, 166.26, 184.73, 221.68 and 240.15). The obtained stability bearing capacity is listed in Table 5. It can be seen from Fig. 9 that with the increase of the nominal slenderness ratio, the stability bearing capacity of the composite column decreases obviously. It can be seen from Table 5 that the stability bearing capacity of the composite column is 3328.21 kN when the nominal slenderness ratio is 110.84 while this value decreases to 771.16 kN (i.e., 76.83% decrease) when the nominal slenderness ratio increases to 240.15, indicating that the nominal slenderness ratio has great influence on the stability of composite columns. In addition, it can be seen from Fig. 9 that with the increase of the nominal slenderness ratio, the curve after the peak load decreases more smoothly, indicating a better the ductility of the column. Therefore, the selection of a reasonable the nominal slenderness ratio is crucial to the safety of the structure.

5.3 Hoop Coefficients (ξ)

The variation of the load–displacement (N-μ_m) curves of the STHCC specimens with hoop coefficients (i.e., 7.60, 8.54, 9.55, 10.61, 11.74 and 12.95) are shown in Fig. 10. The stability bearing capacity of the composite column with different hoop coefficients is listed in Table 6.

It can be seen from Fig. 10 that with the increase of the hoop coefficient, the stability bearing capacity of the composite column increases significantly. For instance, the stability bearing capacity of the composite column increases from 1128.11 to 1389.95 kN with 23.21% increase when the hoop coefficient increases from 7.60 to 12.95 (Table 6). In addition, it can be seen from Fig. 10 that the load–displacement curves seem to be elevated integrally without ductility loss with the increase of hoop coefficient.

Table 5 The stability bearing capacity of specimens

No.	C-6	C-7	C-8	C-9	C-10	C-1	C-11	C-12
λ_t	110.84	129.31	147.78	166.26	184.73	203.20	221.68	240.15
N_{usn} (kN)	3328.21	2527.19	1965.97	1549.62	1267.67	1058.83	908.76	771.16

Fig. 10 The load–displacement (N-μ_m) curves of STHCC specimens with different hoop coefficients

5.4 Flange Width (h_1)

The influences of the flange width on the stability of the STHCC specimens are shown in Fig. 11 and the stability bearing capacity is listed in Table 7. With the increase of the flange width from 120 to 200 mm (l = 11 m), it can be
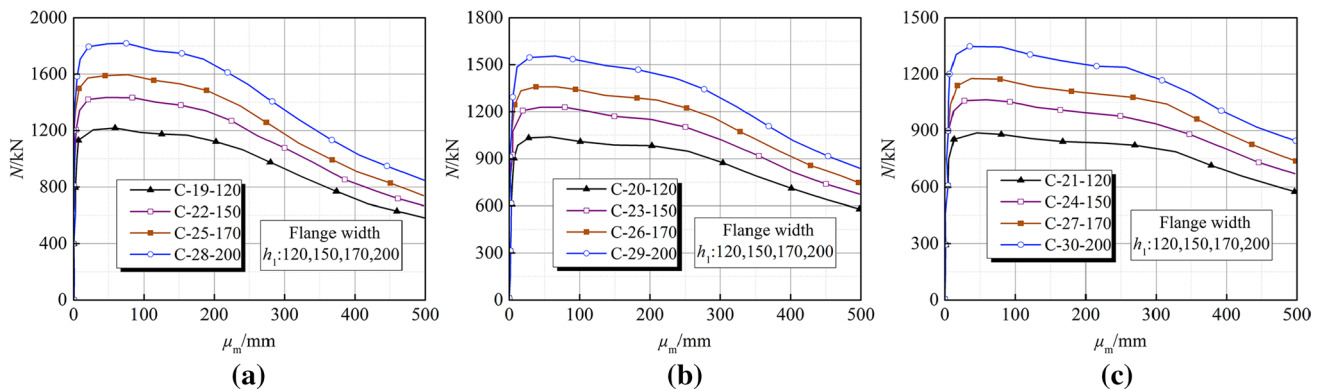
seen from Table 7 that the stability bearing capacity increases from 1215.56 to 1800.92 kN (i.e., 48.16% increase). Therefore, with a constant flange length b, the stability of STHCC is significantly improved with the increase of the flange width.

5.5 Comparison Between Eigenvalue Analysis/ Nonlinear Buckling Analysis and Test Result

Only the von Mises stress nephograms of eigenvalue analysis and nonlinear buckling analysis of specimen C-19 are shown in Fig. 12 for other specimens exhibit the similar von Mises stress nephograms. It can be seen from the Fig. 12a that the deformation of the composite column obtained from the eigenvalue analysis is more uniform and smoother than that of the nonlinear bulking analysis because that the initial imperfection and material nonlinearity are not considered. However, the von Mises stress and buckling capacity are all larger than those of the actual value. In addition, it can be seen from Fig. 12b that the deformation near the ends of the composite column obtained from the nonlinear bulking analysis is relatively smaller while the mid-span deformation is larger compared with those gained from the eigenvalue analysis because of

**Table 6** The stability bearing capacity of specimens

No.	C-13	C-14	C-15	C-16	C-17	C-18
ξ	7.60	8.54	9.54	10.61	11.74	12.96
N_{usn} (kN)	1128.11	1190.78	1235.34	1292.39	1352.47	1389.95

Fig. 11 The load–displacement (N-μ_m) curves of STHCC specimens with different flange width. **a** C-19, 22, 25, 28 (l = 11 m), **b** C-20, 23, 26, 29 (l = 12 m), **c** C-21, 24, 27, 30 (l = 13 m)

Table 7 The stability bearing capacity of specimens

No.	C-19	C-20	C-21	C-22	C-23	C-24
h_1 (mm)	120	120	120	150	150	150
N_{usn} (kN)	1215.56	1041.17	895.35	1444.07	1229.85	1060.27
No.	C-25	C-26	C-27	C-28	C-29	C-30
h_1 (mm)	170	170	170	200	200	200
N_{usn} (kN)	1595.67	1361.05	1175.07	1800.92	1559.07	1346.17
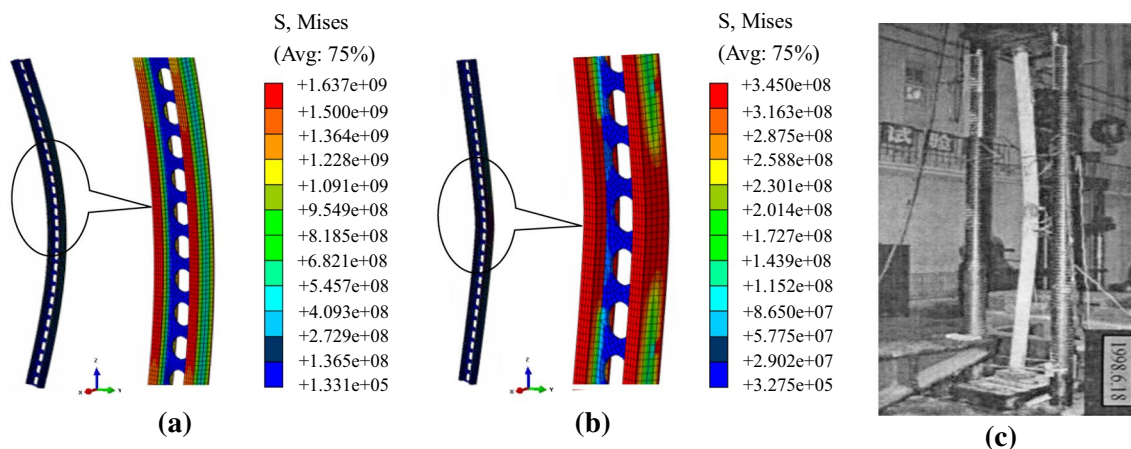
Fig. 12 The deformation diagram obtained from eigenvalue buckling analysis, nonlinear buckling analysis and test. **a** Eigenvalue buckling, **b** nonlinear buckling, **c** Test

Table 8 Simulated value N_{usn} of nonlinear buckling and the composite effect correction value β_c

No.	C-1	C-2	C-3	C-4	C-5	C-6	C-7	C-8	C-9	C-10
N_{usn} (kN)	1058.42	1085.42	1104.18	1114.53	1139.27	3328.21	2527.19	1965.97	1549.62	1267.67
β_c	273.46	247.64	235.16	226.73	249.32	263.11	250.24	276.67	268.50	275.80
No.	C-11	C-12	C-13	C-14	C-15	C-16	C-17	C-18	C-19	C-20
N_{usn} (kN)	908.97	771.16	1128.11	1190.78	1235.34	1292.39	1352.47	1389.95	1215.56	1041.17
β_c	237.41	229.95	239.87	247.54	273.12	229.83	238.16	254.77	170.68	154.28
No.	C-21	C-22	C-23	C-24	C-25	C-26	C-27	C-28	C-29	C-30
N_{usn} (kN)	895.35	1444.07	1229.85	1060.27	1595.67	1361.05	1175.07	1800.92	1559.07	1346.17
β_c	146.31	95.04	97.54	99.53	36.42	46.80	51.05	− 22.43	− 19.16	− 15.28

considering the geometric nonlinearity and material nonlinearity, and is consistent with its actual experimental deformation (Fig. 12c). Therefore, the nonlinear buckling analysis accounting the influence of the initial imperfection can be used to predict the stability of composite column STHCC.

6 Formula for Nonlinear Buckling Load $N_{u, cr}$

6.1 Formula Establishment

The stability capacity N_{usn} of the STHCC column with different parameters predicted through using FE analysis based on 30 specimens (C-1 ~ C-30) is listed in Table 8. A formula is proposed to predict the stability bearing capacity of the composite columns (STHCC) considering the influences of the concrete strength grade, the nominal slenderness ratio, the hoop coefficient and the flange width by superposition method. In addition, the composite effect correction value β_c based on the stability formula of CFST column proposed by Han (2016) is also introduced.

A formula proposed to predict the stability bearing capacity $N_{u, cr}$ of STHCC is expressed as follows:

$$N_{u,\,cr} = \frac{2d}{(\lambda + 35)^2} A_{sc}(1.18 + 0.85\xi)f_{ck} + \frac{\pi^2 k_y EI}{(\mu l)^2} - \beta_c \quad (12)$$

$$d = \left[13500 + 4810 \cdot \ln\left(\frac{235}{f_y}\right)\right] \cdot \left(\frac{25}{f_{ck} + 5}\right)^{0.3} \cdot \left(\frac{\alpha}{0.1}\right)^{0.05} \quad (13)$$

$$\lambda = \frac{2\sqrt{3}l}{b} \quad (14)$$

where, λ is the slenderness ratio of CFST flange; A_{sc} is the cross section area of single CFST flange; ξ is the hoop coefficient; f_{ck} is the standard value of concrete axial compressive strength; f_y is the yield strength of steel; β_c is the composite effect correction value; μ is the calculation length factor; α is the steel content; k_y is the reduction factor of the moment of inertia of the web (Zhang 2008).
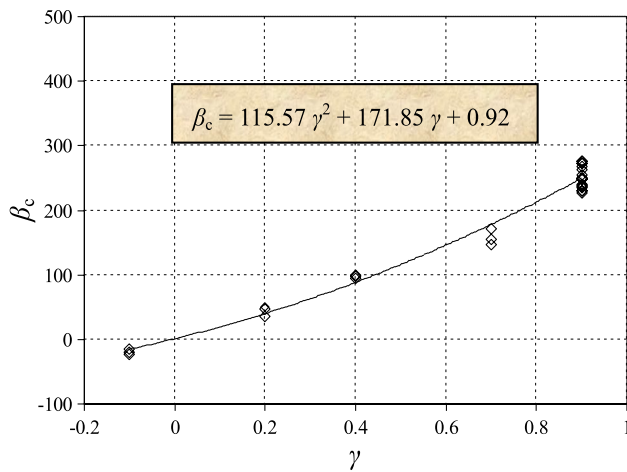
Fig. 13 Relationship between β_c and γ

The composite effect correction values β_c of 30 specimens (C-1 ~ C-30) are obtained by using Eq. 12 (i.e., $N_{usn} = N_{u, cr}$) and the results are listed in Table 8.

The cross section characteristic parameter γ related to the section size of the specimen is introduced, and can be calculated by Eq. 15.

$$\gamma = \frac{(b - h_1 - 10)}{100} \tag{15}$$

As shown in Fig. 13, through statistical regression analysis, the relationship between the composite effect correction value β_c and the cross section characteristic parameter γ is established as Eq. 16.

$$\beta_c = 115.57\left[\frac{(b - h_1 - 10)}{100}\right]^2 + 171.85\frac{(b - h_1 - 10)}{100} + 0.92 \tag{16}$$

where, b is flange length, and h_1 is flange width.

Substituting Eq. 16 into Eq. 12, the formula for predicting the nonlinear stability bearing capacity of STHCC is derived as follows:

$$N_{u, cr} = \frac{2d}{(\lambda + 35)^2}A_{sc}(1.18 + 0.85\xi)f_{ck} + \frac{\pi^2 k_y EI}{(\mu l)^2}$$
$$- \left(115.57\left[\frac{(b - h_1 - 10)}{100}\right]^2 + 171.85\frac{(b - h_1 - 10)}{100} + 0.92\right) \tag{17}$$

6.2 Formula Verification

Lastly, the FE models of other 22 STHCC columns (C-31-C-52) were established to verify the reasonableness of the formula for nonlinear buckling load $N_{u, cr}$. The parameters of the specimens, the simulated value N_{usn} and

Table 9 The comparison of stability bearing capacity of 26 STHCC columns

No.	$h_w \times h_1 \times b \times t_1 \times t_2$ (mm^5)	l (m)	λ_t	ξ	f k cu(MPa)	N_{usn} (kN)	$N_{u, cr}$ (kN)	$|N_{u, cr} - N_{usn}|/N_{usn}$ (%)
C-31	380×100×200×10×20	7	121.24	5.006	40	2555.36	2517.67	1.48
C-32	380×100×200×10×20	8	138.56	5.006	40	1992.15	1992.46	0.02
C-33	380×100×200×10×20	9	155.89	5.006	40	1584.69	1602.09	1.10
C-34	380×100×200×10×20	10	173.21	5.006	40	1299.66	1305.10	0.42
C-35	380×100×200×10×20	12	207.84	5.006	40	922.25	890.46	3.45
C-36	380×100×200×10×20	13	225.17	5.006	40	779.70	742.39	4.79
C-37	380×100×200×10×20	7	121.24	4.005	50	2591.85	2523.18	2.65
C-38	380×100×200×10×20	8	138.56	4.005	50	2026.88	1996.48	1.50
C-39	380×100×200×10×20	9	155.89	4.005	50	1614.38	1609.31	0.31
C-40	380×100×200×10×20	10	173.21	4.005	50	1323.26	1311.26	0.91
C-41	380×100×200×10×20	12	207.84	4.005	50	938.24	894.59	4.65
C-42	380×100×200×10×20	13	225.17	4.005	50	801.74	774.38	3.41
C-43	380×100×200×11×20	7	121.24	3.270	60	2641.20	2523.31	4.46
C-44	380×100×200×12×20	8	138.56	3.270	60	2261.45	2297.33	1.59
C-45	380×100×200×13×20	9	155.89	3.270	60	1644.73	1611.18	2.04
C-46	380×100×200×14×20	10	173.21	3.270	60	1346.54	1313.24	2.47
C-47	380×100×200×15×20	12	207.84	3.270	60	932.77	896.51	3.89
C-48	380×100×200×16×20	13	225.17	3.270	60	807.87	776.19	3.92
C-49	380×120×200×10×20	9	155.89	5.750	30	2350.21	2298.35	2.21
C-50	380×120×200×10×20	10	173.21	5.750	30	1430.75	1446.34	1.09
C-51	380×150×200×10×20	9	155.89	4.865	30	2102.49	2149.98	2.26
C-52	380×150×200×10×20	10	173.21	4.865	30	1724.99	1720.95	0.23

the calculated value $N_{u, cr}$ of nonlinear buckling load are listed in Table 9. It can be seen from Table 9 that the formula outcomes obtained by Eq. 17 has high reliability.

7 Conclusions

A systematic study was conducted on the stability properties of STHCC columns through FE analysis using ABAQUS. Firstly, the correctness of the FE model was verified by comparing with the experimental results conducted by former researchers. Then, the nonlinear buckling analyses of 30 STHCC specimens were carried out to investigate the influences of the concrete strength grade, the nominal slenderness ratio, the hoop coefficient and the flange width on the nonlinear bulking capacity of STHCC columns. A formula considering the above parameters was proposed to predict the nonlinear bulking capacity of STHCC column $N_{u, cr}$ based on the equation proposed by Han for the stability capacity of the CFST columns. Based on the results of FE analyses of the STHCC specimens, the following conclusions can be drawn:

1. The established formula can be used to predict the lower boundary of the stability bearing capacity of STHCC columns, namely the nonlinear buckling load.
2. The STHCC column is deformed along the strong axis of the CFST flange. Therefore, it is effective to improve the stability of the column by connecting the two independent CFST columns into a whole by using connecting plate in practice.
3. When the flange thickness increases from 11 mm to 16 mm (i.e., the corresponding hoop coefficient increases from 7.60 to 12.95), the stability bearing capacity of STHCC column increased by 23.21%. Hence, the stability of the column can be improved by increasing the thickness of the flange appropriately.
4. With the increase of concrete strength grade, the improvement of the stability capacity of STHCC column is slight.

References

ABAQUS Inc. (2006). *ABAQUS analysis user s manual*. Palo Alto: ABAQUS Inc.

BSEN1993-1-1. (2005). *Eurocode 3: Design of steel structures-Part 1-1: General rules and rules for buildings*. London: British Standards Institution.

Ellobody, E., & Ghazym, F. (2012). Experimental investigation of eccentrically loaded fibre reinforced concrete-filled stainless steel tubular columns. *Journal of Constructional Steel Research, 76*(2), 167–176.

GB50010-2010. (2014). *Code for design of concrete structures*. Beijing: China Building Industry Press.

Han, L. H. (2016). *Concrete-filled steel tubular structures: Theory and practice*. Beijing: Science Press. **(in Chinese)**.

Hassanein, M. F., & Silvestre, N. (2013). Lateral–distortional buckling of hollow tubular flange plate girders with slender unstiffened webs. *Engineering Structures, 56*(6), 572–584.

James, M. G., & Barry, J. G. (2011). *Strength of materials*. Beijing: Machinery Industry Press.

Ji, J., Xu, Z. C., et al. (2017). Eigenvalue buckling analysis of H-type honeycombed composite column with rectangular concrete-filled steel tube flanges. *Journal of Northeast Petroleum University, 41*(1), 106–116. **(in Chinese)**.

Ji, J., Zhang, W. F., et al. (2018). Finite element model based test and analysis on ACHC short columns and hoop coefficient. *Cluster Computing, 21*(1), 1–13.

Lama, D., & Gardner, L. (2008). Structural design of stainless steel concrete filled columns. *Journal of Constructional Steel Research, 64*(11), 1275–1282.

Li, W. (2011). *Study on the seismic performance of circular concrete-filled steel tubular column to steel beam joint with external diaphragm*. Doctor Dissertation, Tsinghua University, Beijing **(in Chinese)**.

Liang, W. F. (2016). *Experimental research on global stability behavior of I-beams with top flange of rectangular concrete-filled steel tube*. Master Dissertation, Northeast Petroleum University, Daqing **(in Chinese)**.

Patton, M. L., & Singh, K. D. (2017). Buckling of fixed-ended concrete-filled steel columns under axial compression. *International Journal of Steel Structures, 17*(3), 1059–1071.

Ren, Y. W. (2015). *Experimental and theoretical investigation of bending behavior for rectangular steel tube flange beams*. Master Dissertation, Northeast Petroleum University, Daqing **(in Chinese)**.

Yang, Y., Zhou, J., et al. (2016). Experimental study on the compression of concrete filled steel tubular latticed columns with variable cross section. *Steel & Composite Structures, 22*(3), 663–675.

Yu, Z. W., & Ding, F. X. (2003). Unified calculation method of compressive mechanical properties of concrete. *Journal of Building Structures, 24*(4), 41–46.

Zhang, Y. F. (2008). *Global and local stability analysis of cellular beams*. Master Dissertation, Central South University, Changsha **(in Chinese)**.

Zhang, W. F., Liu, Y. C., et al. (2014). Analysis of dynamic behavior for truss cable structures. *Steel & Composite Structures, 16*(2), 117–133.

Zhang, W. F., Liu, Y. C., et al. (2016). Lateral-torsional buckling analysis of cantilever beam with tip lateral elastic brace under uniform and concentrated load. *International Journal of Steel Structures, 16*(4), 1161–1173.

Zheng, W. Z., & Ji, J. (2008a). Dynamic performance of angle-steel concrete columns under low cyclic loading-I: Experimental study. *Earthquake Engineering and Engineering Vibration, 7*(1), 67–75.

Zheng, W. Z., & Ji, J. (2008b). Dynamic performance of angle-steel concrete columns under low cyclic loading-II: Parametric study.

Earthquake Engineering and Engineering Vibration, 7(2), 137–146.

Zhong, S. T. (2010). *The concrete-filled steel tubular structures*. Beijing: Tsinghua University Press. **(in Chinese)**

Zhou, T. (2012). *Mechanical behavior and engineering application of special-shaped column composed of concrete-filled square steel tubes*. Doctor Dissertation, Tianjin University, Tianjin **(in Chinese)**.